


Mechanisms of Zhixiao Tang on Anti-Inflammatory Multiple Targets and Multiple Components: Metabonomics Combined with Database Mining Technology

Kaiyue Zhang , Chunnan Li, Peitong Wu, Xiaochen Gao, Xueqin Feng, Jiaming Shen, Nanxi Zhang, Xuesheng Hu, Shuo Wang, Hui Zhang, Jingwei Lv, Jiaming Sun

Jilin Ginseng Academy, Changchun University of Chinese Medicine, Changchun, Jilin, People's Republic of China

Correspondence: Jiaming Sun; Jingwei Lv, Changchun University of Chinese Medicine, No. 1035, Boshuo Road, Nangan District, Changchun, 130117, People's Republic of China, Tel +0431-86763809, Fax + 8676 3968, Email Sun_jiaming2000@163.com; jingwei-lv@hotmail.com

Purpose: Zhixiao Tang (ZXT), a traditional Chinese compound prescription, has been used clinically to treat pneumonia in China. However, the underlying mechanism of ZXT treatment in pneumonia is still unclear. The present study aimed to reveal the potential mechanism of ZXT in pneumonia using a strategy combining metabolomics and network pharmacology.

Methods: Initially, the chemical compositions were identified by UPLC-QE-Orbitrap-MS, while the prediction of potential signal pathways was performed through network pharmacology. To assess the anti-inflammatory properties of ZXT in the context of pneumonia, models of 16HBE cells induced by LPS and zebrafish induced by CuSO₄ were established to measure levels of inflammatory markers and apoptosis. Subsequently, the differential changes of endogenous metabolites in cells caused by ZXT were examined using metabolomics technology, and the molecular docking analysis of key targets was carried out using Autodock Vina software. Ultimately, the validation of the primary pathways and targets was conducted through quantitative RT-PCR and Western blot techniques.

Results: A total of 75 compounds were identified through UPLC-QE-Orbitrap-MS analyses. Network pharmacological analysis shows that it plays an anti-inflammatory role in C-type lectin receptor signaling pathway. After ZXT intervention, the inflammatory factors and apoptosis in cells were significantly reduced. Metabonomics analysis showed that 18 metabolites changed significantly. Four key genes were identified, which exhibited partial compatibility with the findings of network pharmacology. Molecular docking analysis confirmed the substantial affinity of the primary targets for ZXT. Furthermore, ZXT exerted a suppressive effect on neutrophil migration, down-regulated the expression of pro-inflammatory cytokine genes, and inhibited the up-regulation of the Dectin-1/SYK/NF-κB signaling pathway. In vivo cell experiments also yielded consistent experimental outcomes.

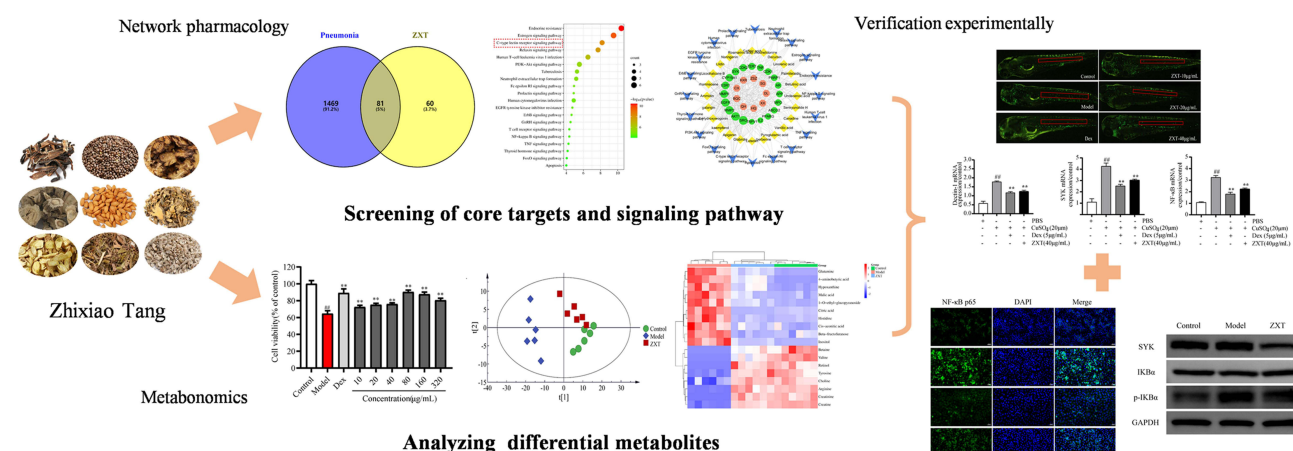
Conclusion: This study enhances comprehension of the pharmacological mechanism underlying ZXT's efficacy in pneumonia treatment, thereby establishing a scholarly basis for future research and clinical utilization of ZXT in pneumonia management.

Keywords: Zhixiao Tang, pneumonia, network pharmacology, integrated metabolomics, 16HBE, Zebrafish

Introduction

Pneumonia is an acute lower respiratory tract infection that primarily affects the lungs. Upon entry into the host, the pathogen will directly infiltrate the respiratory tract, resulting in the disruption of bronchial epithelial cells and impeding ciliary motility.¹ Consequently, this leads to the impairment of respiratory defense mechanisms and the initiation of pneumonia through neutrophil phagocytosis. In recent years, the escalating morbidity and mortality rates have significantly impacted individuals' overall well-being and both their physical and mental health. Lipopolysaccharide (LPS), a bioactive constituent of endotoxin, serves as the principal component of the cell wall in Gram-negative bacteria, and

Graphical Abstract



plays a pivotal role in eliciting inflammatory responses.² LPS can directly or indirectly initiate pathophysiological mechanisms within host cells. Consequently, LPS has emerged as the prevailing model for inducing inflammation.

Zhixiao Tang (ZXT), an empirical prescription formulated by Professor Lie Wang, a national tutor, in accordance with the fundamental principles of Traditional Chinese Medicine (TCM), has been employed for the management of pneumonia since the 1970s at the Affiliated Hospital of Changchun University of Chinese Medicine. ZXT consists of *Pheretima aspergillum* (E. Perrier) (“Di-long” in Chinese, DL), *Ligusticum chuanxiong* Hort. (“Chuan-xiong” in Chinese, CX), *Perilla frutescens* (L.) Britt. (“Zi-su-zi” in Chinese, ZSZ), *Belamcanda chinensis* (L.) DC. (“She-gan” in Chinese, SG), *Peucedanum praeruptorum* Dunn (“Qian-hu” in Chinese, QH), *Prunus armeniaca* L. var. *ansu* Maxim. (“Ku-xing-ren” in Chinese, KXR), *Scutellaria baicalensis* Georgi (“Huang-qin” in Chinese, HQ), *Chelidonium majus* L. (“Bai-qu-cai” in Chinese, BQC), *Dictamnus dasycarpus* Turcz. (“Bai-xian-pi” in Chinese, BXP). Owing to the efficacy of “heat-clearance and anti-inflammation” in the theory of traditional Chinese medicine, ZXT is applicable to treat a variety of diseases, including the protective effects on pneumonia and asthma. However, the molecular mechanisms underlying the therapeutic effects of ZXT in the treatment of pneumonia have yet to be fully elucidated. Consequently, there is an urgent need to conduct further investigations into the mechanism of action of ZXT, with the aim of facilitating its subsequent advancement and utilization. (The human data involved in this study were exempted from approval in accordance with the nationally mandated legislative guidelines for Ethical Review of Life Science and Medical Research Involving Human Subjects).

Metabolomics’ study of holistic metabolic properties in complex biological matrices is consistent with the holistic thinking of Chinese medicine and can be used to explore the pathological mechanisms of airway inflammation in pneumonia and the efficacy of Chinese medicines.^{3,4} The application of metabolomics in the treatment of pneumonia with Chinese medicine has been reported, mainly in animal and human samples.⁵ Animal models can partially simulate the pathological changes of pneumonia, but their species differences with humans pose many hidden dangers for clinical translation. Cellular metabolomics, however, utilizes human cell models to effectively detect endogenous cellular metabolites, thereby accurately reflecting the biomarker information pertaining to cellular life activities.⁶ Consequently, this approach unveils the metabolic pathways and processes of the relevant cells, rendering it highly valuable for in vitro investigations concerning alterations in metabolic profiles and the underlying mechanisms induced by pharmaceutical interventions.⁷ In comparison to comprehensive metabolic investigations, cellular metabolomics offers distinct advantages, including the ability to easily regulate experimental variables, achieve high reproducibility, incur low costs, and facilitate result interpretation. Zebrafish (*Danio rerio*) possesses exceptional attributes such as its diminutive size, prolific reproduction, economical upkeep, brief experimental duration, and substantial homology with mammals,

particularly humans. Consequently, zebrafish has gained significant popularity as a model organism for studying human diseases and as a tool for drug discovery in the past decade.⁸ Zebrafish disease models are extensively employed across diverse disciplines within the life sciences, encompassing immunology, oncology, and notably, zebrafish is regarded as an exemplary inflammatory model for the discovery of novel drugs exhibiting enhanced anti-inflammatory properties, owing to the resemblance of its immune system to that of humans.⁹

The present study employed Ultra performance liquid chromatography-Q Exactive hybrid quadrupole mass spectrometry (UPLC-QE-Orbitrap-MS) to analyze the chemical composition of ZXT. Subsequently, network pharmacology methods and metabolomics approaches were utilized to predict the key targets and pathways associated with the treatment of ZXT pneumonia. Finally, the anti-inflammatory effects of ZXT on 16HBE and zebrafish, along with their underlying mechanisms, were investigated. These findings establish a scientific foundation for the utilization of this drug in pneumonia treatment.

Materials and Methods

Experimental Instruments and Reagents

Pheretima aspergillum (E. Perrier), *Ligusticum chuanxiong* Hort, *Perilla frutescens* (L.) Britt., *Belamcanda chinensis* (L.) DC., *Peucedanum praeruptorum* Dunn, *Prunus armeniaca* L.var.ansu Maxim, *Scutellaria baicalensis* Georgi, *Chelidonium majus* L, *Dictamnus dasycarpus* Turcz were collected from Anhui Yuankang Traditional Chinese Medicine Decoction Pieces Co., Ltd., (Anhui, China) and authenticated by Professor Sun Jiaming (Changchun University of Chinese Medicine). Reference standards (purity > 98%) of caffeic acid, apigenin, kaempferol, berberine, rhamnacene and luteolin were purchased from Shanghai source leaf Biological Technology Co., Ltd. (Shanghai, China).

Enzyme-linked immunosorbent assay (ELISA) kits for quantifying the concentrations of IL-6 and TNF- α were procured from Dakewe (Beijing, China). Dexamethasone (Dex) was generously supplied by Tianxin (Guangzhou, China). Lipopolysaccharide (LPS), dimethyl sulphoxide (DMSO), 3-[4,5-dimethylthiazol-2-yl]-2,5-diphenyltetrazoliumbromide (MTT) and various other reagents were acquired from Sigma-Aldrich (St Louis, USA).

Preparation of ZXT Extract

The decoction was prepared by soaking 2.5 g of KXR and 10 g of other herbs in water at the ratio of material to liquid of 1:10 (g/mL) for 30 min, heating and reflux for 1 h, and collecting the decoction. An equal amount of water was then added to the residue and reflux was repeated for 1 h. The components were combined, filtered, concentrated under reduced pressure to a crude drug content of 1 g/mL, and lyophilized to obtain loose powder.

Weigh precisely 1.32 mg of ZXT lyophilized powder and add 1 mL of methanol to achieve the desired volume. Subject the mixture to ultrasonic treatment for a duration of 30 min, followed by cooling to room temperature. Subsequently, add methanol to the mixture and pass it through a 0.22 μ m filter membrane. Finally, refine the obtained filtrate to obtain a volume of 5 μ L, which will be used for instrument detection.

Standard Solution Preparation

The reference compounds were accurately measured and dissolved in methanol to generate standard stock solutions, which were subsequently refrigerated at 4°C prior to analysis. The working solutions were subsequently prepared by diluting the stock solutions with methanol.

UPLC-QE-Orbitrap-MS Analysis Conditions

The samples underwent separation using the poroshell 120 EC-C₁₈ column (250 mm x 4.6 mm, 4.0 μ m; Waters, Milford, MA, USA) with a flow rate of 0.4 mL/min and a column temperature of 35°C. The mobile phase consisted of 0.1% formic acid aqueous solution (mobile phase A) and acetonitrile (mobile phase B). Gradient elution was performed as follows: 0~20 min, 2~49% B; 20~30 min, 49~90% B; 30~55 min, 90~100% B.

Electrospray ionization sources were employed in both positive (ESI⁺) and negative (ESI⁻) ion modes, utilizing a scan range spanning from m/z 66.7–1000. The MS source parameters were configured as follows: a sheath gas flow rate

of 35 L/min, an auxiliary gas flow rate of 15 L/min, a scan gas flow rate of 1 L/min, a gas temperature of 350°C, and a capillary voltage of 3.5kV. The scan mode is Full MS/dd-MS²(Top N, N=8) with resolutions of 70000 (Full MS) and 17500 (dd-MS²), respectively. Xcalibur software (Thermo Fisher Scientific) was used for data recording and analysis.

Identification of Compounds

The characteristic peaks were extracted by Compound Discoverer software, and identified by HMDB database (<http://www.hmdb.ca/>) and mzCloud database (<https://www.mzcloud.org/>). The screening criteria were as follows: the best match score > 80. The mass spectrometric information of the screened target compound was compared with that of the reference substance and relevant literature, for compound analysis and identification.

Network Pharmacological Analysis

Target Prediction

The standard Canonical SMILES format of each compound was stored in the PubChem database, with the species specified as “Homo Sapiens”. The Swiss Target Prediction database (<http://www.swisstargetprediction.ch/>) was utilized to obtain the targets associated with each compound,¹⁰ and the proteins with high confidence ($p > 0$) were selected and the duplicates were removed. Log in to the platforms of Online Mendelian Inheritance in Man (OMIM, <https://www.omim.org/>),¹¹ Genecards (<https://www.genecards.org/>),¹² and Therapeutic Target Database (TTD, <https://db.idrblab.net/ttd/>),¹³ and enter the keyword “pneumonia” to screen that the p value is greater than 0.5, which is standardized by Uniprot (<https://www.uniprot.org/>),¹⁴ and the weight is removed after merger. The Venny (<https://bioinfo.gp.cnb.csic.es/tools/venny/index.html>) was employed to identify the overlapping targets between the ZXT component targets and the targets associated with pneumonia disease.

Construction and Analysis of Target PPI Network

Higher scores in the String database (<https://cn.string-db.org/>) indicate greater confidence in protein interactions.¹⁵ Protein-protein interactions (PPI) at intersecting targets were analyzed using String database. The results were imported into cytoscape software, and the nodes with high scores in the network were obtained by using CytoNCA plug-in. By intersecting three values greater than the mean, degree, closeness and betweenness, key targets were identified.

Function Annotation and Pathway Analysis

The gene ontology (GO) function annotation and Kyoto Encyclopedia of Genes and Genomes (KEGG) pathway analysis were conducted using the Metascape database (<http://metascape.org/gp/index.html#/main/step1>) to analyze the primary targets of ZXT. The threshold $p < 0.05$ was set, and the biological function processes of the top 10 items and the signaling pathways of the top 20 items were selected for visualization.

Construction of “Drug Flavor-Component-Core Target-Pathway” Network

Cytoscape 3.8.0 software (Boston, MA, USA) was used to establish the interaction network diagram of “drug flavor-component-core target-pathway”, and the main active components of ZXT in treating pneumonia were analyzed by Network Analyzer function.

Metabolomics Analysis

Cell Culture

The 16HBE human bronchial epithelial cells (American Type Culture Collection, Rockville, USA) were cultured in DMEM (Thermo Fisher Scientific, Waltham, USA) supplemented with 10% (v/v) FBS. The cells were maintained at a temperature of 37 °C and a CO₂ concentration of 5%.¹⁶

Cell Viability Assay

The MTT assay has been extensively employed for the evaluation of cellular viability. Cells in logarithmic phase were taken and spread evenly at 2×10^4 cells /mL in 96-well plates (200 μ L per well). After pre-incubation for 24 h, divided

into the control group, model group (1 µg/mL LPS), positive group (25 µg/mL Dex), and drug group (10, 20, 40, 80, 160 and 320 µg/mL), and incubation was continued for 24 h. Each well was added with 10 µL of 5 mg/mL MTT solution. After 4 h, 150 µL DMSO was dissolved and the absorbance value was measured at 490 nm to calculate the cell viability. Cell viability = $A_s/A_c \times 100\%$, A_c is the absorbance value of the control group and A_s is the absorbance value of the drug group.

Enzyme-Linked Immunosorbent Assay (ELISA)

The protein levels of Interleukin-4 (IL-4), Interleukin-13 (IL-13) and Tumor Necrosis Factor- α (TNF- α) in the cell supernatants were quantified using an ELISA kit, following previously established protocols. In summary, cells were pre-treated with LPS for 24 h, followed by stimulation with specified concentrations of 80 µg/mL ZXT for an additional 24 h. Subsequently, the levels of IL-4, IL-13 and TNF- α were assessed according to the instructions provided by the manufacturer.

Cell Apoptosis

16HBE cells were plated into 6-well plates with a density of 2×10^5 cells and 2 mL of medium per well. After overnight culture, the drug medium was replaced and the cells were kept for 24 h. Refer to Annexin V-FITC Apoptosis Detection Kit for operation.

Cellular Interventions

Take logarithmic growth phase 16HBE cells and inoculate them in culture flasks at a density of 1×10^7 cells per bottle. Set up a control group, a model group, and ZXT group, and incubate them at 37°C with 5% CO₂ for 24 h. Once the cells have attached to the wall and are in a good growth state, replace the serum-free medium. At the same time, add a final concentration of 1 µg/mL LPS to the model group and ZXT group, respectively, and continue to cultivate them for 24 h. Add 80 µg/mL samples to the ZXT group and collect the cells from each bottle after continuing to cultivate for 24 h. After centrifugation in PBS, the supernatant was promptly quenched in liquid nitrogen. Each group was set up with 6 parallel groups, and the collected cells in each bottle were cultured for 24 h. The cells were washed twice with PBS centrifugation, and after discarding the supernatant, they were rapidly quenched in liquid nitrogen and stored at -80°C overnight.

Cellular Metabolomics Sample Preparation

The cells were removed, and a mixture of methanol and water (1:2, v/v) was added. The mixture was then vortex and subjected to ice bath ultrasonic crushing treatment, with ultrasonication set to run for 5 s, pause for 9 s, and repeat this cycle 85 times. This treatment ensured complete dissolution of the cell contents. Subsequently, the cell crushing solution was centrifuged at 4°C and 13,000 rpm/min for 10 min. The resulting supernatant was transferred to a nitrogen blowing apparatus to remove the methanol solvent. The solution was then lyophilized and prepared for further use.

The lyophilized powder of the cell was dissolved in 600 µL of PBS solution, which contained 0.005% TSP-d₄. Subsequently, the resulting solution was subjected to centrifugation at a temperature of 4°C and a speed of 13,000 revolutions per minute for a duration of 10 min. The supernatant obtained after centrifugation was then transferred into a 5 mm NMR tube, specifically designed for analysis on a Bruker 600-MHz AVANCE III spectrometer. TSP-d₄ was utilized as the internal standard during the analysis. The NOSEY sequence was employed, with a relaxation delay of 320 ms, a spectral width of 12,019.12 Hz, and a total of 64 scans.

The raw NMR files underwent processing using MestReNova software. Following positioning, baseline calibration, and normalization, the NMR spectra were integrated within the δ 0-9 region at uniform intervals of δ 0.04, excluding the δ 4.80–5.06 range corresponding to residual water peaks. The resulting integrated data were then imported into an Excel spreadsheet for systematic arrangement.

Multivariate Statistical Analysis

In order to evaluate the variations in cellular metabolites among the control, model, and drug groups, the obtained results were subjected to Principal Component Analysis (PCA), Partial Least Squares Discriminant Analysis (PLS-DA), and Orthogonal Partial Least Squares Discriminant Analysis (OPLS-DA) utilizing SIMCA software (Version 14.1).

Differential metabolites were identified by combining a VIP value greater than 1 in the S-plot plot of OPLS-DA and the independent samples test, which was conducted at a significance level of $p < 0.05$. The identification of differential metabolites was conducted using the HMDB database (<http://www.hmdb.ca/>). Subsequently, the screened differential metabolites were subjected to clustering analysis, and volcano plots were generated. Furthermore, the relevant metabolic pathways were analyzed using MetaboAnalyst 5.0 (<https://www.metaboanalyst.ca/MetaboAnalyst/>).

Molecular Docking Analysis

The 3D structure of the active components in ZXT was visualized using ChemDraw software (version 12.0, CambridgeSoft, Cambridge, MA, USA). The protein structures of rac-alpha serum/threonine-protein kinase (AKT1, PDB ID:6npz), proto-oncogene tyrosine-protein kinase Src (SRC, PDB ID:3d7t), tyrosine-protein kinase SYK (SYK, PDB ID:4xz0), and type IV collagenase (MMP2, PDB ID:7xgj) were obtained from the RCSB PDB database (<https://www.rcsb.org/>).¹⁷ The molecules were docked using AutoDock Vina, followed by the selection of the appropriate conformation and the plotting of the 3D binding pattern using PyMOL.

Experimental Verification

Immunofluorescence Detection

Immunofluorescence staining was employed to detect the expression of NF- κ B in bronchial epithelial cells (16HBE). Cells treated with LPS or/and ZXT were sectioned for a duration of 24 h, followed by staining with a primary antibody, specifically rabbit anti-NF- κ B (dilution ratio of 1:100), and incubated for 12 h at a temperature of 4°C. The sections were then washed three times with PBS and subsequently stained with donkey anti-goat Cy3 (dilution ratio of 1:500) for a duration of 30 min at room temperature. Nuclei were counterstained using DAPI, and the fluorescence emitted by the samples was captured using confocal laser scanning microscopy.

Western Blot Analysis

Well-grown 16HBE cells were collected and inoculated into 6-well plates with 2×10^5 cells per well. After 24 h of culture, the cells were treated with 80 μ g/mL of ZXT. Total cellular proteins were extracted from the cell lysate on ice, and the protein concentration was determined using the BCA method. SDS-PAGE electrophoresis was performed, transferred to a 0.22 μ m PVDF membrane, and incubated at room temperature with 5% BSA for 1 h. The primary antibodies used in this study were GAPDH (1:2000), SYK (1:1000), I κ B α (1:1000), and pI κ B α (1:1000). These antibodies were incubated overnight at 4°C, followed by a 1XTBST wash for 30 min. Subsequently, a secondary antibody (1:5000) was applied and incubated at room temperature for 1 hour. Another 1XTBST wash for 30 min was performed. The development of colors was achieved using an ECL luminescent solution, and gel imaging system was utilized to capture images. The gray values of the bands were then analyzed and quantified using ImageJ software.

Zebrafish Maintenance and Embryos Collection

In accordance with established maintenance protocols, transgenic zebrafish Tg(MPX:EGFP) were reared under a 14 h light/10 h dark photoperiod within a recirculating aquatic habitat system, maintaining a salinity range of 0.03%–0.04%. These zebrafish were provided with a diet consisting of either dry food or brine shrimps, which were administered three times daily. The present study obtained approval from the Animal Ethics Committee of Changchun University of Chinese Medicine (approval No.2021369), and all animal experiments adhered to the regulations outlined in the Administration of Experimental Animals of Changchun University of Chinese Medicine and the Animal Protection Law of the People's Republic of China.

During the experiment, adult zebrafish were introduced into breeding tanks overnight, with a male-to-female ratio of 1:2. The embryos spawned at the onset of the light period were carefully gathered into a sterile Petri dish filled with egg water containing 0.002% methylene blue for the purpose of sterilization. Subsequently, these embryos were kept in an incubator set at a temperature of 28.5°C for the subsequent experimental procedures.

Toxicity of ZXT in Zebrafish

Zebrafish embryos at the first day post fertilization (dpf) were subjected to random allocation into a 24-well plate ($n = 20$) and subsequently exposed to varying concentrations of ZXT (ranging from 0 to 250 $\mu\text{g/mL}$). The culture medium was refreshed on a daily basis, and deceased embryos were documented and eliminated at 24 h intervals until the sixth dpf.

Survival Analysis

The zebrafish larvae that had perished were extracted and quantified within the time frame of 0–72 h after injection in order to illustrate the survival patterns.

CuSO₄-Induced Inflammation in Zebrafish

A total of 3 dpf post-fertilization zebrafish larvae were placed in a 24-well plate, with 20 larvae per well. Subsequently, they were subjected to an exposure of 20 μM of CuSO₄, either with or without varying concentrations of ZXT, for a duration of 2 h. Dex at a concentration of 5 $\mu\text{g/mL}$ was employed as the positive control. The recruitment of neutrophils was then observed using an MVX10 fluorescence microscope (Olympus, Tokyo, Japan).

RT-PCR Analysis

A total of 30 whole larvae were used for RNA extraction at 12 h post-infection (hpi) using RNAiso Plus. The subsequent synthesis of first-strand complementary deoxyribonucleic acid (cDNA) was performed using the PrimeScript™ RT reagent Kit with gDNA Eraser. The reverse transcription parameters were set as follows: 37°C for 15 min to initiate the reaction, 85°C for 5 s to deactivate enzymatic activity, and 4°C for preservation. The RT-PCR analysis was performed using the TB Green™ Premix Ex Taq™ II reagent on a LightCycler® 96 real-time PCR instrument manufactured by Roche in Switzerland. The experimental procedure consisted of several sequential steps: an initial denaturation at 95°C for 30s, followed by 50 cycles of amplification at 95°C for 5s and 60°C for 30s, and a final extension at 95°C for 5s, 65°C for 60s, and 95°C for 1s. The expression ratio of the target genes was determined using the $2^{-\Delta\Delta C_t}$ method, with normalization to the expression level of β -actin. The sense and antisense primers provided below were employed in the conducted experiment.

β -actin: ATGGATGAGGAAATCGCTG and ATGCCAACCATCACTCCCTG;
IL-4: AACTCTCTGCCAAGCAGGAA and GCAGTTTCCAGTCCCGGTAT;
IFN- γ : CTCGCATGCAGAATGACAGC and TCGTTTTCTTGTATCGCCCA;
IL-13: GCCTGAAGTGTGAGCATGATT and TTGTCTGGTACGGAAAGGGTC;
TNF- α : GCTGGATCTTCAAAGTCGGGTGTA and TGTGAGTCTCAGCACACTTCCATC;
Dectin-1: TGGGTACCATGGGGTTCTT and CCCAGTTGCCAGCATTTGTCT;
NF- κ B p65: GAGCCCTTTGTGCAAGAGAC and TGGGATACGTCTCCTGTTTC;
SYK: AGAACTCCTGAACTGGCAGC and GAGGAGCGCTAACAACCGTA.

Statistical Analysis

A minimum of five independent experiments were conducted, and the outcomes were reported as the mean \pm standard deviation. Microsoft Excel and GraphPad Prism 8.0.2 software were utilized for data collection and analysis. To assess the significance of the treatment effects based on ZXT dosage, a one-way analysis of variance (ANOVA) was performed.

Results

ZXT Component Analysis

The total ion flow diagrams of ZXT in both positive and negative ion modes are depicted in [Figure 1](#). A total of 75 compounds originating from ZXT were effectively identified through precise mass number determination, retention time analysis, examination of cleavage behavior, comparison with controls, and review of pertinent literature ([Table S1](#)). These compounds encompassed 19 flavonoids, 6 terpenoids, 17 alkaloids, 16 organic acids, 6 coumarins, and 11 other constituents.

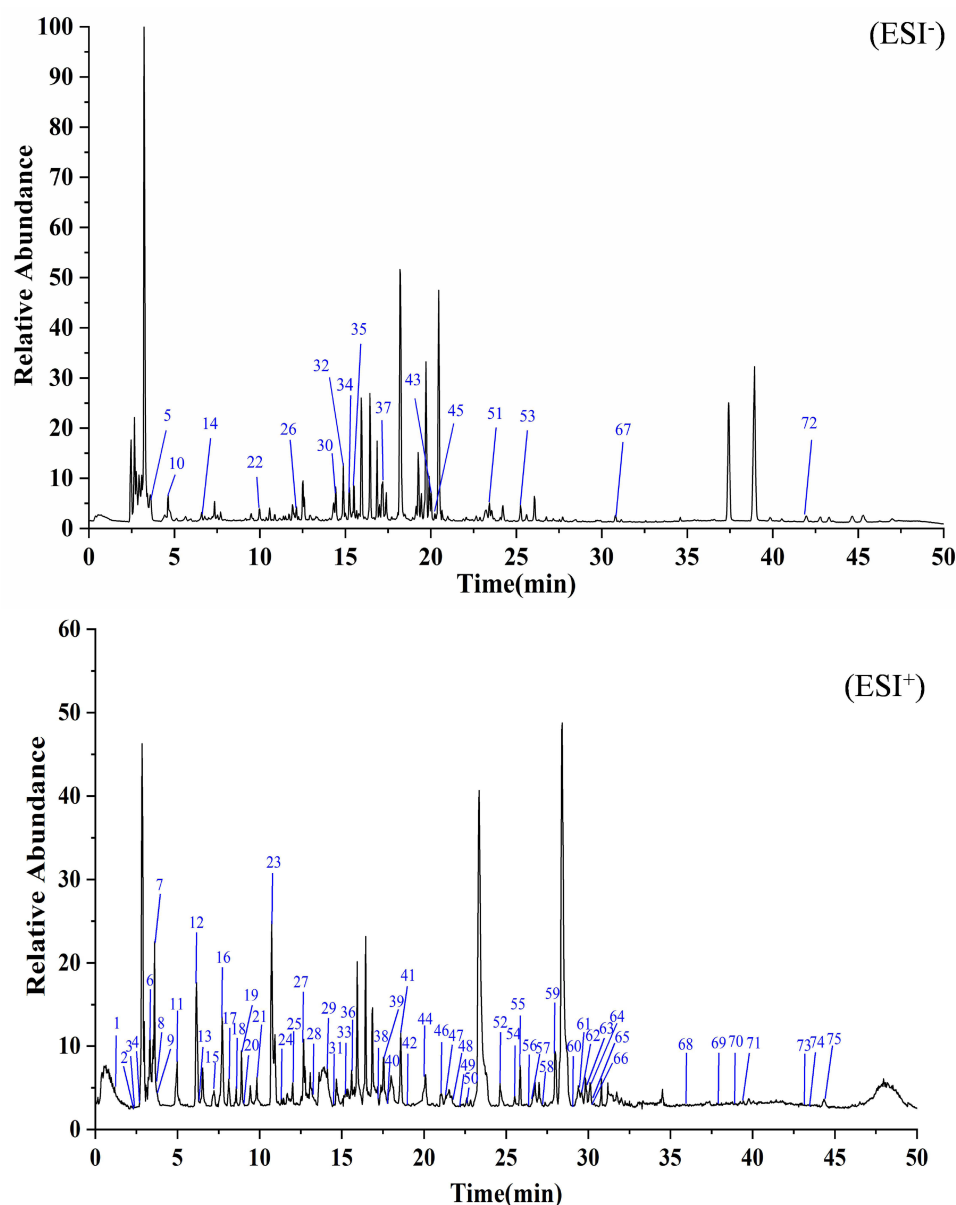


Figure 1 These samples were detected using UPLC-QE-Orbitrap-MS in negative ions mode and in positive ions mode.

Network Pharmacological Analysis

Target Prediction and Analysis of PPI

There were 75 components found in ZXT based on MS analysis, which are considered potential bioactive components. 141 targets associated with these components were collected by SwissTargetPrediction from databases. A comprehensive search across the OMIM, Genecard, and Drugbank databases yielded a collective count of 1551 disease gene targets associated with pneumonia (Figure 2A). Notably, all of these targets were found to be shared among 81 genes (Figure 2B), subsequently facilitating their integration into the String website for subsequent analysis of protein-protein interaction networks and target identification (Figure 2C). Based on the degree>10.5569, betweenness>20.2783 and closeness>0.0060 value, 20 key gene targets are screened out. As shown in Figure 2D, there were bigger nodes for such targets as AKT1, TNF, SRC, EGFR, PPARG, and MMP2, indicating that these targets played a greater role in the network. As a result, they may be the key genes that ZXT targets in treating pneumonia.

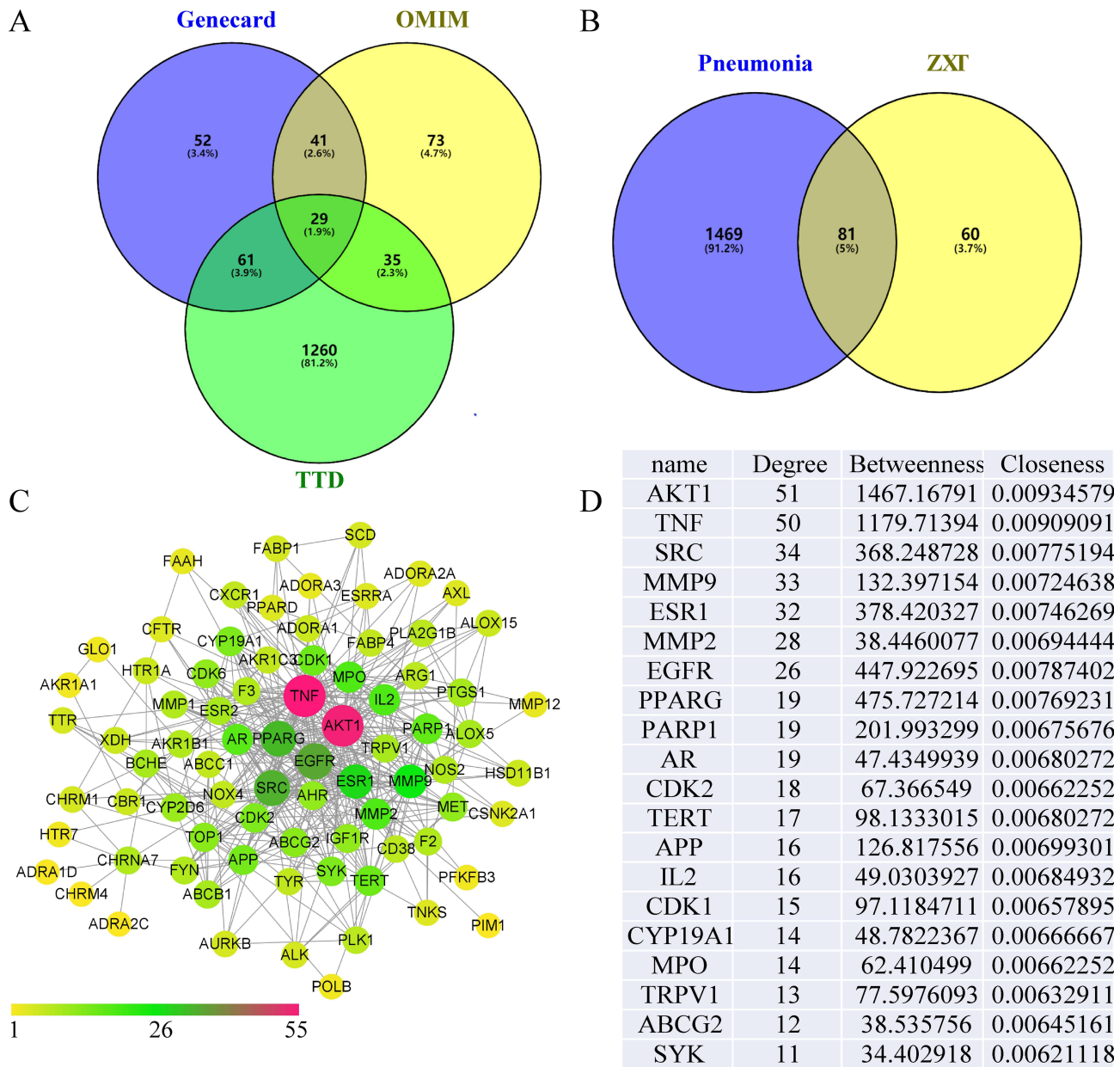
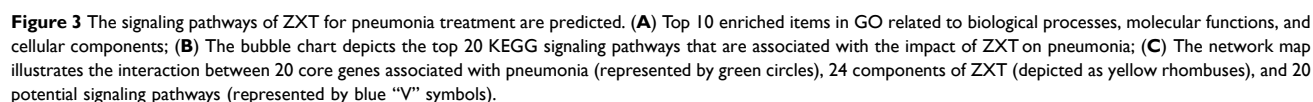


Figure 2 Network pharmacology analysis of ZXT on pneumonia. **(A)** Prediction of pneumonia disease targets. **(B)** Venn diagram of targets between ZXT and pneumonia. **(C)** PPI network diagram. **(D)** Top 20 potential targets for ZXT.

The Potential Signaling Pathways of ZXT for the Treatment of Pneumonia

A statistical analysis revealed that a significant total of 179 GO items were acquired ($p < 0.05$). These items were further categorized into 131 items for biological functional process (BP), 18 items for cell composition (CC), and 30 items for molecular function (MF), constituting proportions of 75.7%, 10.05%, and 16.75%, respectively. The p-value analysis reveals that the top 10 items in terms of BP, CC, and MF are cellular response to chemical reactions, membrane rafts, and receptor binding activity. These findings suggest a potential association between these biological processes and the pathological progression of pneumonia, as depicted in Figure 3A. Metascape was used to predict the achievement of significant abundant signaling pathways at 20 key gene targets. The KEGG enrichment analysis revealed a significant association between numerous target genes and key signaling pathways, including the Fc epsilon RI signaling pathway, T cell receptor signaling pathway, C-type lectin receptor signaling pathway, and TNF signaling pathway (Figure 3B). Notably, these signaling pathways play crucial roles in cellular processes such as inflammation, immunity, and apoptosis.^{18–20}



Effect of ZXT on I6HBE Cells Induced by LPS on Proliferation

Effects of ZXT on the Levels of IL-4, IL-13 and TNF- α in LPS-Induced I6HBE Cells

The model group exhibited a statistically significant elevation ($p < 0.01$) in the levels of diverse inflammatory factors in the cell culture supernatant when compared to the control group. Conversely, the presence of inflammatory factors with

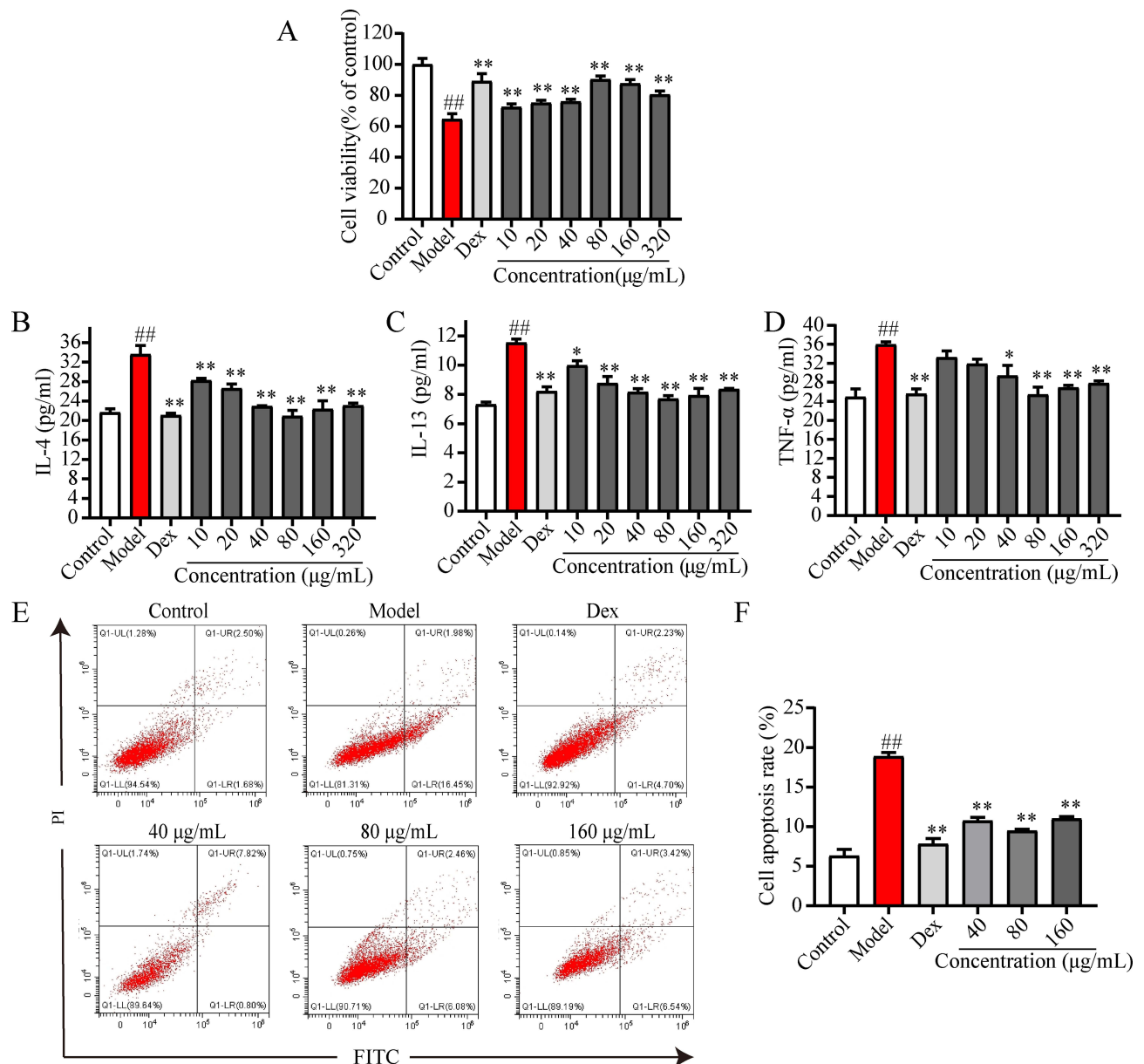


Figure 4 Effect of ZXT on 16HBE cells induced by LPS. **(A)** Proliferation of 16HBE cells treated with ZXT for 24 h. **(B-D)** Effects of ZXT on the release of pro-inflammatory cytokines IL-4, IL-13 and TNF-α. **(E, F)** The cell apoptosis was detected by flow cytometry. Data are presented as the mean ± standard deviation (n = 5) ^{##}*p* < 0.05 and ^{##}*p* < 0.01 versus the control group; ^{*}*p* < 0.05 and ^{**}*p* < 0.01 versus the model group.

varying concentrations of the drug demonstrated a significant reduction ($p < 0.05$). These findings indicate that ZXT possesses the capacity to diminish the levels of inflammatory factors in 16HBE cells and alleviate the inflammatory response (Figure 4B-D).

Cell Apoptosis

The flow cytometry results demonstrated a statistically significant elevation in apoptosis within the model group when compared to the control group ($p < 0.01$). Conversely, the introduction of various concentrations of ZXT exhibited a noteworthy decrease in apoptosis in comparison to the model group ($p < 0.01$) (Figure 4E and F). Consequently, the concentration of 80 μg/mL was determined to be the most effective dosage of ZXT for pneumonia treatment and was subsequently selected for the metabolomics investigation.

Metabolomics Analysis

¹H-NMR Pattern Designation and Attribution of I6HBE Cells

Through the comprehensive examination of chemical shifts, coupling constants, and peak shapes for each compound, in conjunction with referencing literature reports and utilizing the HMDB database for experimental profile identification, a total of 47 compounds were successfully identified. The chemical shifts and corresponding peaks of these compounds are presented in Table 1. These compounds can be classified into various categories including organic acids (such as lactic acid, creatine, citric acid), amino acids (including aspartic acid, alanine, glycine, histidine, leucine, glutamic acid,

Table 1 Attribution of Major Metabolite Peaks in the ¹H-NMR Profiles of I6HBE Cell Samples

No.	Metabolite	δ _H
1	Bile acid	0.73(s)
2	Pantothenic acid	0.90(m), 0.94 (m)
3	Isoleucine	0.94 (t, J = 7.41Hz), 1.01 (d, J = 7.01Hz), 1.98(m)
4	Butyric acid	0.94 (t, J = 8.87Hz), 1.56 (m), 2.16 (t)
5	Leucine	0.95 (s), 1.71 (m), 3.72 (m)
6	Valine	1.01 (d), 1.04 (d), 2.26 (m), 3.6 (d)
7	Ethyl alcohol	1.19 (t)
8	3-hydroxybutyrate	1.20 (d, J=6.6 Hz), 3.33 (d, J=4.8 Hz)
9	1-O-ethyl-β-D-glucopyranoside	1.20 (t, J = 7.0Hz), 3.65 (m)
10	Lipid	1.22(m), 2.00 (m)
11	Lactic acid	1.33(m), 4.11 (m)
12	Alanine	1.44 (d, J = 8.57Hz), 3.77 (d, J = 7.23Hz)
13	Arginine	1.71 (m)
14	4-aminobutyric acid	1.96(m), 2.29 (t)
15	Retinol	1.89(t), 4.18 (d), 6.51(s)
16	Acetamide	1.99(s)
17	Proline	2.01 (m), 2.36 (m), 3.45(m)
18	Glutamic acid	2.04 (m), 2.12 (m), 2.36(m), 3.75(m)
19	Glutamine	2.13 (m), 3.77 (m)
20	Acetoacetic acid	2.28(s)
21	Malic acid	2.38(m), 2.59 (m), 4.07 (m)
22	Carnitine	2.40(m), 4.56(m), 3.41(m), 3.25(s)
23	Citric acid	2.55 (d), 2.65 (d)
24	Aspartic acid	2.67 (dd), 2.82 (m), 3.90 (m)
25	3-Aminoisobutyric acid	3.02 (t, J = 7.2Hz), 2.4 (td, J = 7.2, 2.4Hz)
26	Creatinine	3.03 (s), 4.05 (s)
27	Creatine	3.06 (d), 3.94 (s)
28	Malonic acid	3.12(s)
29	Histidine	3.14 (dd), 3.25 (dd), 3.98 (dd), 7.08 (s), 7.83 (s)
30	Cis-aconitic acid	3.17(s)
31	Lipid	3.2(s)
32	Choline	3.2(s), 3.52 (m), 4.07 (m)
33	Phosphorylcholine	3.23 (s)
34	Betaine	3.27(s), 3.91 (s)
35	Phenylalanine	3.28 (m), 7.33 (d), 7.38 (t)
36	Inositol	3.28 (t, J = 9.0Hz), 3.54 (dd, J = 3.0, 6.6Hz), 3.63 (t, J = 9.6Hz), 4.07 (t, J = 3.0Hz)
37	β-fructofuranose	3.44(m), 3.40 (m)
38	Glycine	3.55 (s)
39	Glucuronic acid	5.62(q), 5.97 (d), 7.95 (d)
40	Guanosine	5.9(s)

(Continued)

Table 1 (Continued).

No.	Metabolite	δ_H
41	Uridine	5.90(m), 7.88 (d)
42	Tyrosine	6.90 (s), 7.20 (s)
43	Aminohippuric acid	6.91(d), 7.71 (d)
44	Benzoic acid	7.48(t), 7.87 (d)
45	l-methylhistamine	8.03(s), 7.11(s), 3.27(m), 3.94(t), 3.73(s)
46	Hypoxanthine	8.22(s), 8.24 (s)
47	Adenosine	8.23(s), 8.35 (s)

phenylalanine, proline, etc)., fatty acids (such as butyric acid, malonic acid), organic bases (such as betaine, etc)., and other compounds (such as inositol, tetra phosphoric acid glycerol).

LPS-Induced Changes in the Metabolic Profile of I6HBE Cells

The Simca-P software was utilized to process the data, and the parameters of various models are presented in Table 2. Unsupervised PCA was employed to analyze the ^1H -NMR metabolic profiles of all cell samples, with the outcomes displayed in Figure 5A. The PCA results revealed a clear distinction between the control group and the model group, indicating a significant alteration in the metabolic state of LPS-induced I6HBE cells. Additional analysis utilizing the PLS-DA pattern recognition technique (Figure 5B) revealed distinct differentiation between the control group and the model group, thereby corroborating the findings of the PCA analysis and affirming the successful replication of the LPS inflammatory cell model. The model validation results indicated that the R^2 and Q^2 values on the left side were consistently lower than those of the original points on the right side, providing evidence for the high reliability of the constructed model. Additionally, a notable observation was made regarding the scatter points of I6HBE cells treated with ZXT, as they exhibited significant separation from those of the model group. This finding suggests that ZXT possesses the ability to mitigate LPS-triggered inflammation, as depicted in Figure 5C.

Intervention of ZXT on LPS-Induced Metabolism in I6HBE Cells

In order to further elucidate disparities in endogenous metabolites within I6HBE cells, the samples underwent analysis utilizing OPLS-DA and OPLS-DA score plots, followed by the creation of corresponding S-plot loading plots (Figure 6A and B). Differential metabolites were sought through the integration of S-plot plots with $\text{VIP} > 1$ and independent samples t -test $p < 0.05$. A total of 18 metabolites exhibiting noteworthy variations in peak area were successfully identified. ZXT intervention resulted in significant up-regulation of valine, arginine, choline, betaine, retinol, and tyrosine, while 4-aminobutyric acid, hypoxanthine, histidine, malic acid, 1-O-ethyl- β -D-glucoside, inositol, and β -fructofuranose were significantly down-regulated compared to the model group (Figure 6C).

Metabolic Pathway Analysis

The above differential metabolites were imported into MetaboAnalyst 5.0 (<https://www.metaboanalyst.ca/MetaboAnalyst/>) for pathway analysis. Metabolic pathways with impact > 0.1 were used as potential target pathways.

Table 2 Analysis of Different Models and Their Parameters

Model	Type	A	N	R^2X	R^2Y	Q^2	Title
Model 1	PCA	3	18	0.879	–	–	Total
Model 3	PLS-DA	2	12	0.805	0.981	0.941	Model/Control
Model 4	PLS-DA	2	12	0.937	0.939	0.882	ZXT/Model
Model 5	OPLS-DA	2	12	0.763	0.986	0.924	Model/Control
Model 7	OPLS-DA	2	12	0.941	0.975	0.896	ZXT/Model

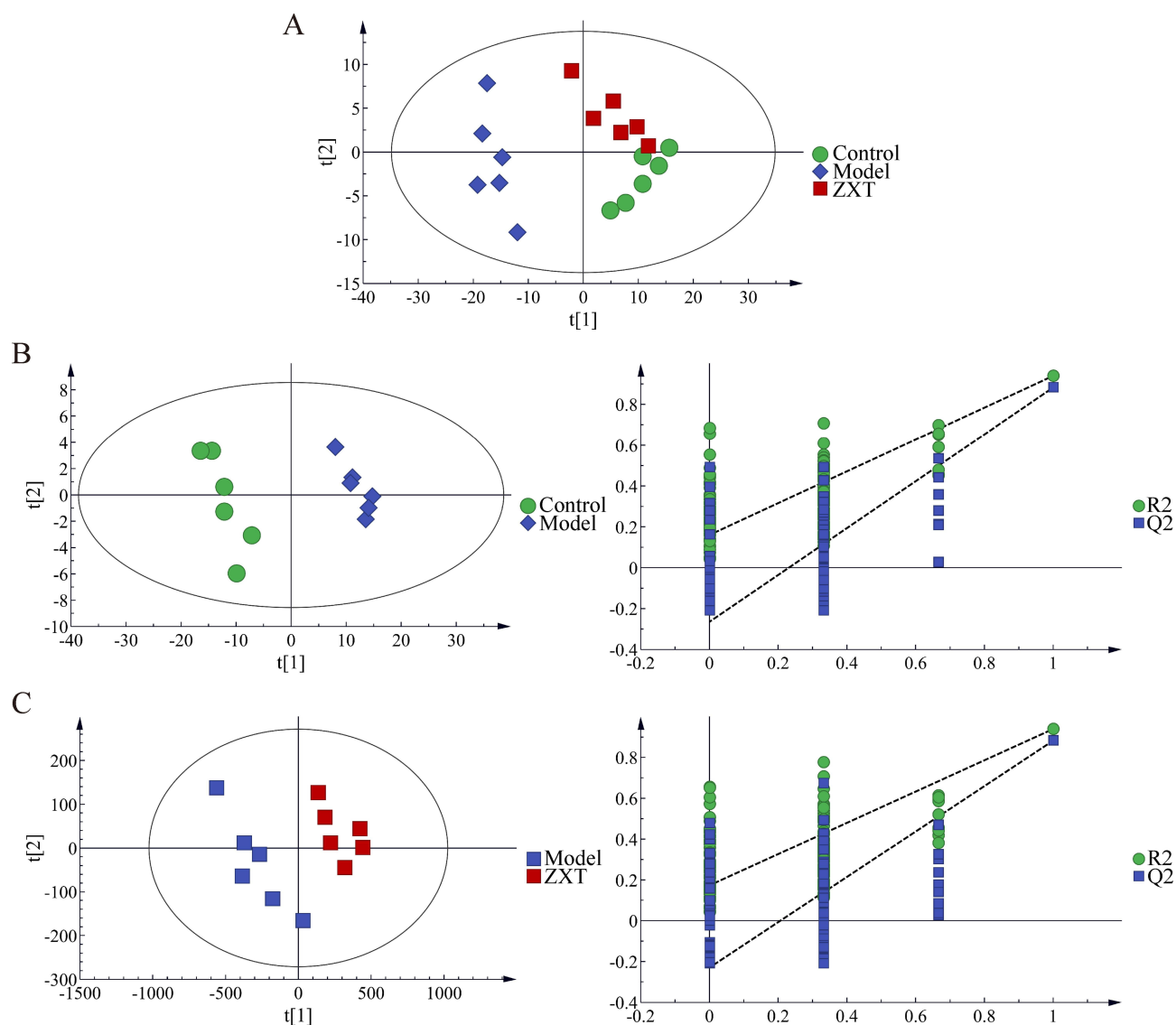


Figure 5 PCA scatter plot of I6HBE cells (A), PLS-DA scatter plot of control and model group and corresponding model validation (B) and scatter plot of ZXT and model group and corresponding model validation (C).

The results showed that eight metabolic pathways were significantly altered: aminoacyl tRNA biosynthesis, alanine, aspartate and glutamate metabolism, glyoxylate and dicarboxylic acid metabolism, glycine, serine and threonine metabolism, arginine and proline metabolism, the citric acid cycle (TCA cycle), and the biosynthesis of phenylalanine, tyrosine and tryptophan to D-glutamine and D-glutamate metabolism (Figure 7), these metabolic pathways are mainly involved in protein biosynthesis, amino acid metabolism, and energy metabolism.

Analysis of Metabolic Targets Related to Potential Biomarkers

A comprehensive set of 240 metabolic targets was successfully identified through the utilization of Cytoscape, with a reliance on putative biomarkers as depicted in Figure 8. Surprisingly, by combining the results of the pharmacological analysis of the ZXT network, four cross-targets were found among the metabolic targets, ZXT targets, and pneumonia targets, which were AKT1, SRC, MMP2, and SYK, and were worthy of further investigation.

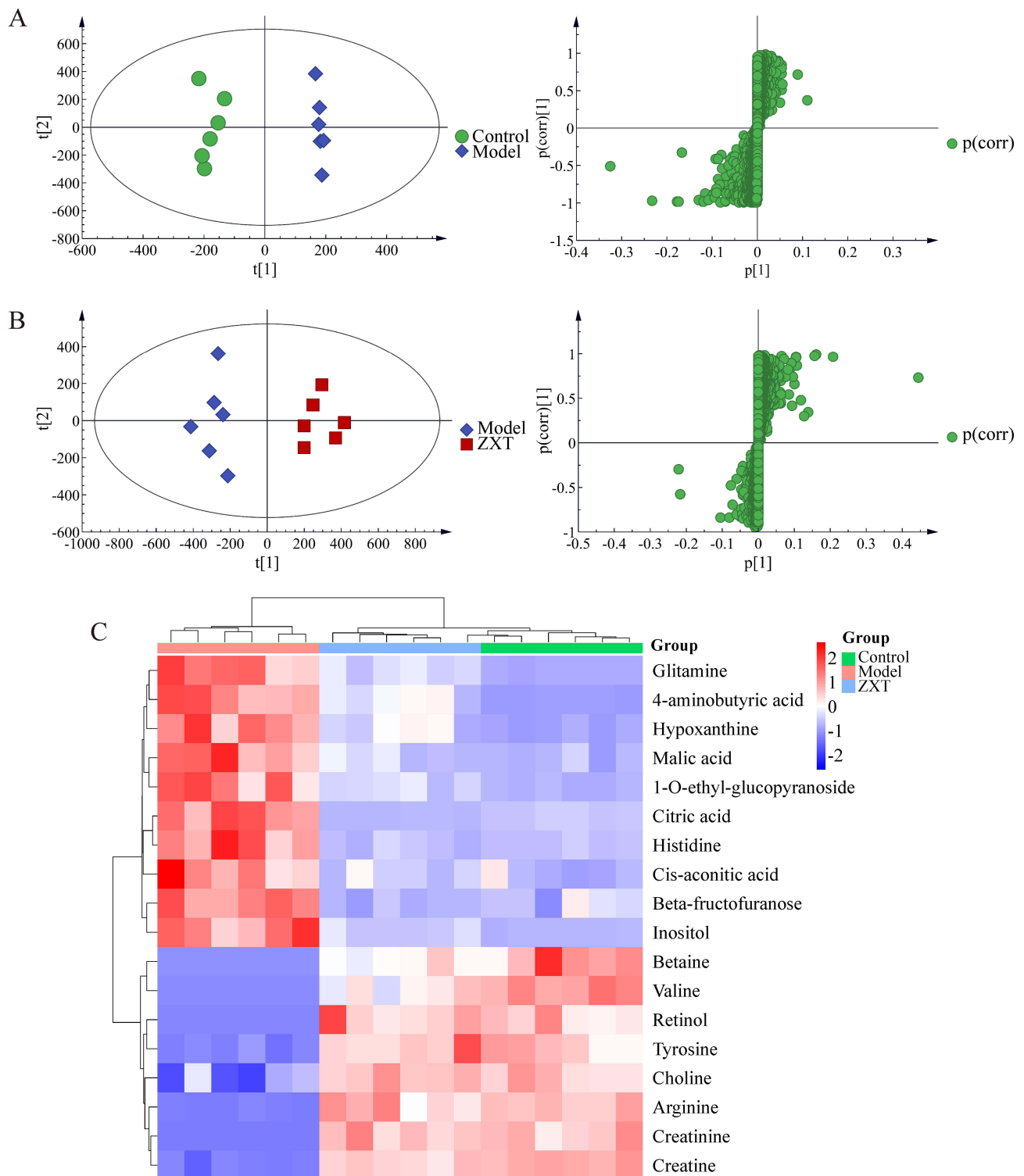


Figure 6 OPLS-DA scatter plots (A), corresponding S-plot plots (B) and differential metabolite heat maps (C) of samples from the control, model group and ZXT group.

Docking Analysis

Molecular docking is a technique employed to determine the most likely conformation of a ligand within the active site of a receptor, as well as to estimate the binding energy.²¹

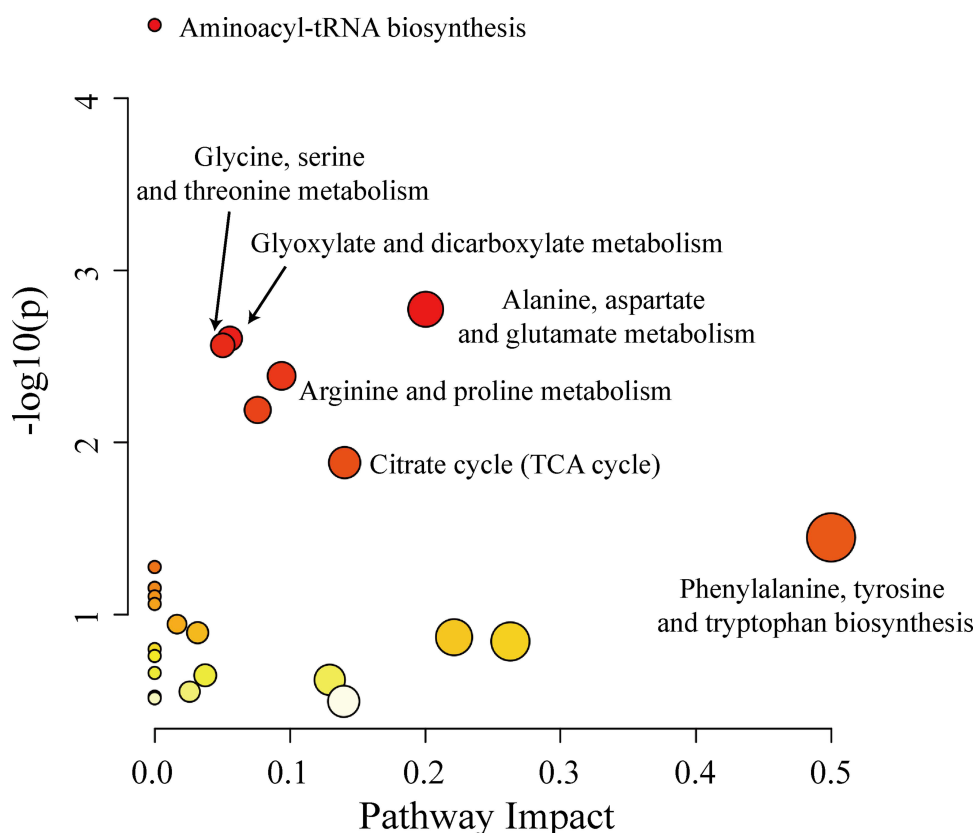


Figure 7 Metabolic pathway analysis.

Molecular docking is more effective when the binding energy is low. Based on the above results, AKT1, SRC, MMP2, and SYK were the key targets of ZXT in the treatment of pneumonia. Molecular docking analysis of the four targets and their associated components showed that ammidin, apigenin, and glabridin were the main active components, as shown in Figure 9A and B. The observed binding energy between the ligand compound and the receptor protein was found to be less than -6 kcal/mol, indicating a strong affinity of these components towards the AKT1, SRC, MMP2, and SYK proteins.

Experimental Validation Analyses

Effect of ZXT on LPS-Stimulated NF- κ B Nuclear Translocation in I6HBE Cells

The activation of NF- κ B signaling by LPS results in the induction of IL-4 expression, thereby initiating an inflammatory response. Thus, inhibition of NF- κ B signaling reduced the production of pro-inflammatory cytokines. It was found that green fluorescence represented NF- κ B staining, while blue fluorescence represented nuclear staining, as shown in Figure 10. NF- κ B entry into the nucleus was detected by immunofluorescence, and in the blank group, NF- κ B was mainly expressed in the cytoplasm. However, NF- κ B was distributed in both the nucleus and cytoplasm. In comparison to the control group, the cells in the experimental group exhibited evident nuclear translocation as a result of injury and heightened release of Th2-type cytokines, accompanied by a notable increase in NF- κ B expression within the nucleus and enhanced nuclear co-localization. Conversely, when compared to the experimental group, the presence of NF- κ B within the nucleus was significantly diminished upon treatment with 80 μ g/mL ZXT.

ZXT Inhibits the Activation of Dectin-1 and SYK in LPS-Induced I6HBE Cells

To further elucidate the mechanism of action of ZXT in the treatment of pneumonia, we conducted immunoblot analysis to assess the protein levels of SYK, I κ B α and pI κ B α in I6HBE cells. The Western blot data revealed that treatment with ZXT significantly suppressed the phosphorylation of I κ B α and the expression of Dectin-1 and SYK in I6HBE cells.

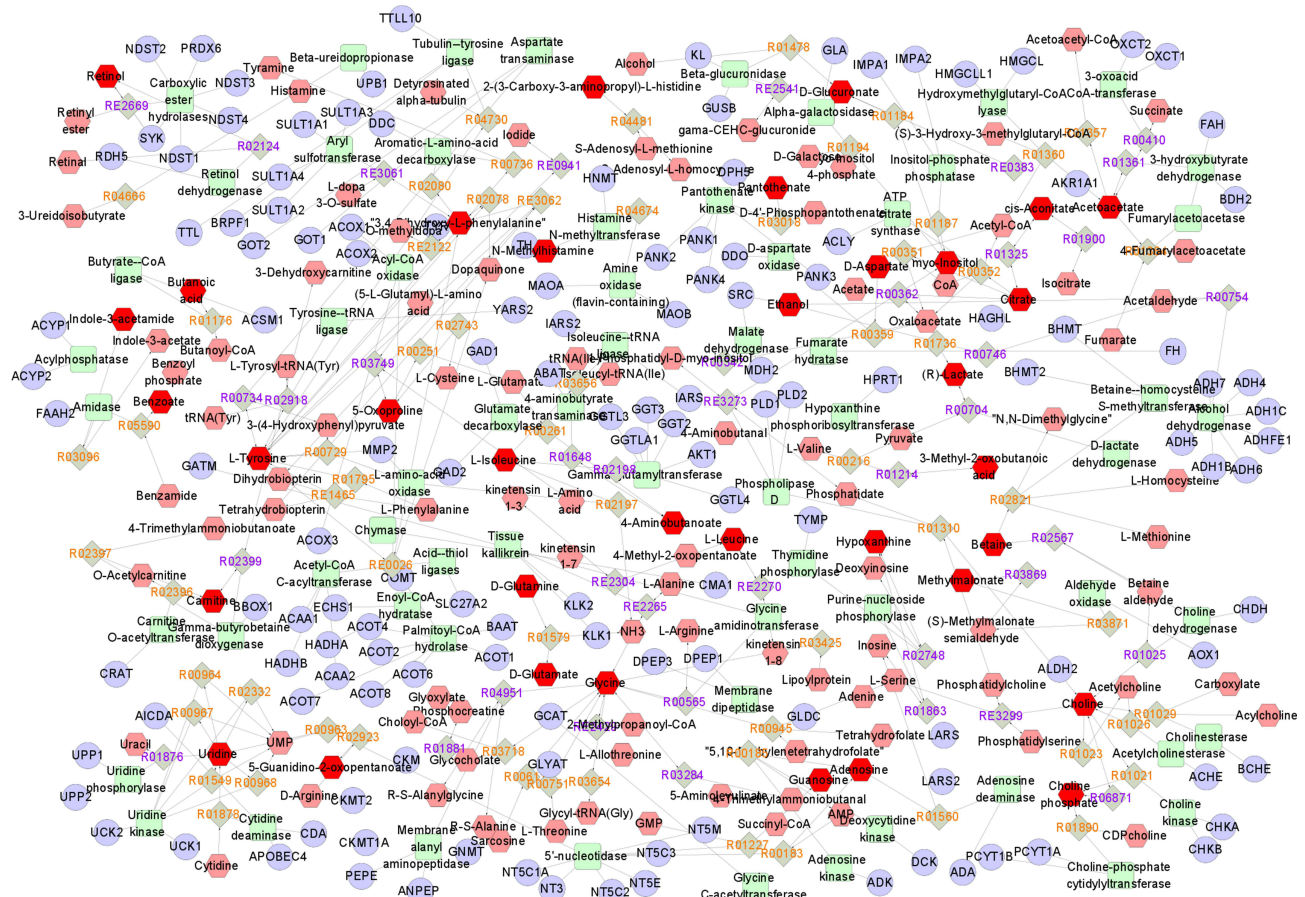


Figure 8 Metabolic targets are based on potential biomarkers.

induced by LPS (Figure 11). These findings indicate that ZXT has the ability to inhibit the activation of SYK and NF- κ B in 16HBE cells stimulated by LPS.

ZXT Protects the Zebrafish Challenged by CuSO₄

In order to assess the potential toxicity of ZXT in zebrafish, the researchers observed the morphological alterations and mortality rates of zebrafish larvae exposed to various concentrations of ZXT on a daily basis. Figure 12A demonstrates that concentrations ranging from 10–40 μ g/mL, which exhibited survival rates exceeding 95%, were deemed non-toxic and thus suitable for subsequent applications.

To visually investigate the *in vivo* defense effect of ZXT, juvenile fish at 3 dpf were subjected to CuSO₄·5H₂O (20 μ M) to induce lethal inflammation. The results revealed that ZXT exhibited the ability to enhance the survival rate of zebrafish, with a comparable trend to that of Dex treatment at a concentration of 40 μ g/mL (Figure 12B).

Effects of ZXT on the CuSO₄-Induced Inflammation Model

As depicted in Figure 12C and D), the number of immune cells in zebrafish that migrated in the model group was significantly higher ($p < 0.01$) compared to the control group, suggesting that exposure to CuSO₄ solution induced an inflammatory response in zebrafish. Conversely, the number of immune cells in the positive control group and ZXT treatment groups was significantly lower than that in the model group ($p < 0.01$). Furthermore, the reduction in the number of immune cells in the ZXT treatment groups was found to be dose-dependent, indicating the anti-inflammatory activity of ZXT.

ZXT Exerts Its Anti-Inflammatory Effect via the Inhibition of c-Type Lectin Receptor Signaling

In order to elucidate the mechanism by which ZXT exerts its anti-inflammatory effect *in vivo*, we conducted a qRT-PCR analysis to assess the impact of ZXT on the expression of proinflammatory cytokines IL-4, IFN- γ , IL-13, and TNF- α in

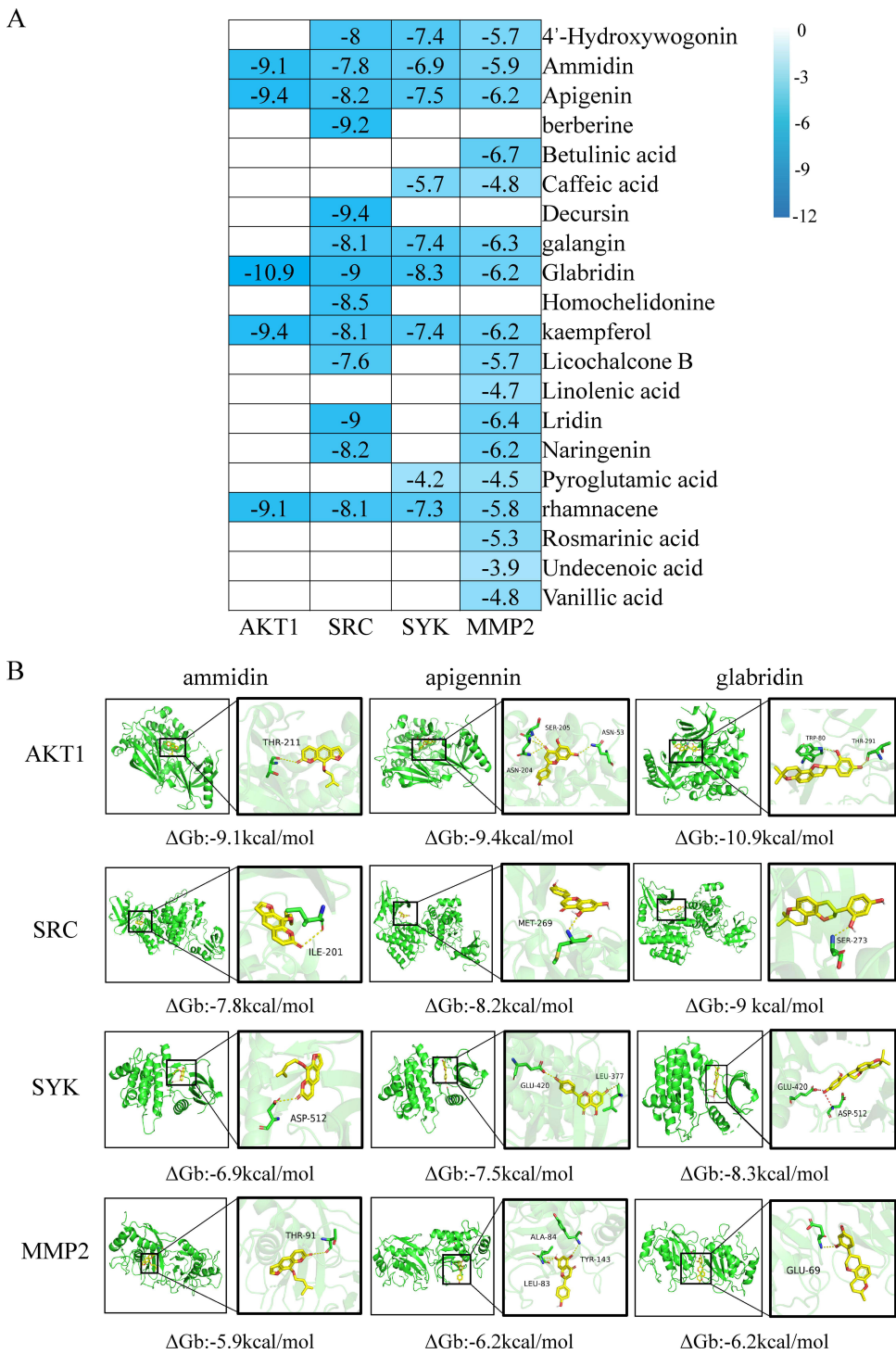


Figure 9 Molecular docking analyze. **(A)**The molecular docking binding energy between the twenty active components and the four core targets. **(B)** A docking diagram showing the relationship between ammidin, apigenin, and glabridin with genes from the KEGG pneumonia core pathway (AKT1, SRC, SYK, and MMP2).

CuSO₄-induced zebrafish. Our results indicate that ZXT effectively inhibits the release of IL-4, IFN- γ , IL-13, and TNF- α in vivo, as supported by statistically significant findings (Figure 12E). To further investigate the potential involvement of the c-type lectin receptor signaling pathway in the in vivo anti-inflammatory effect of ZXT, we conducted gene expression analysis of Dectin-1, a constituent of the C-type lectin receptor family, as well as the central target SYK and the downstream factor NF- κ B. ZXT demonstrated significant inhibition of the upregulation of Dectin-1, SYK, and NF- κ B p65 in zebrafish

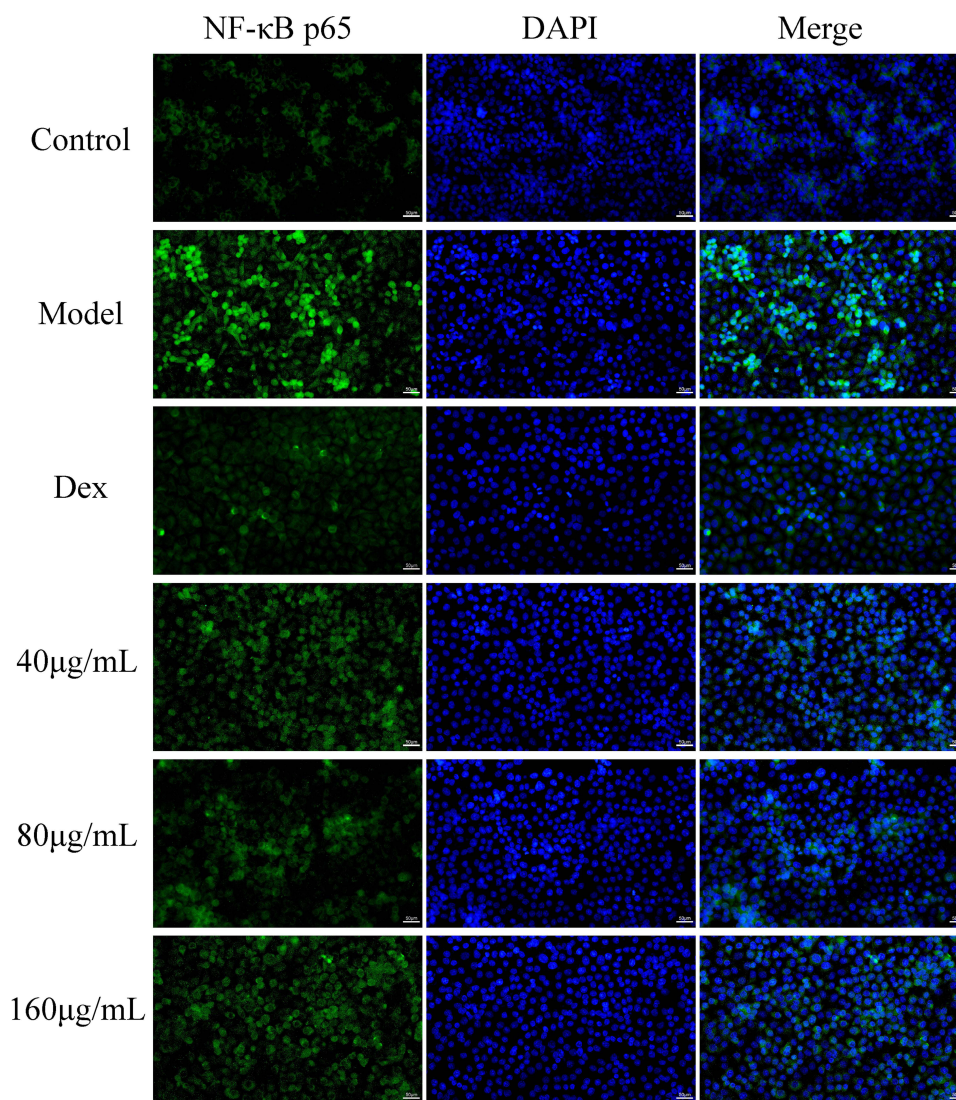


Figure 10 Effect of ZXT on NF-κB nuclear translocation in 16HBE cells.

induced by CuSO_4 . This suggests that the anti-inflammatory effects of ZXT, particularly in the regulation of IL-13 and $\text{TNF-}\alpha$ expression, are partially mediated by the inhibition of the Dectin-1/SYK/NF-κB in CuSO_4 -stimulated zebrafish.

Discussion

The clinical use of the traditional herbal formulation, ZXT, as a treatment for pneumonia has been established for several decades. However, there is a dearth of documented information regarding its underlying mechanism of action in the management of this respiratory ailment.²² The complex composition of herbal medicines presents a formidable obstacle in investigating their active components and potential mechanisms. Consequently, this study employed UPLC-QE-Orbitrap-MS to conduct a qualitative analysis of the constituents present in ZXT. A comprehensive analysis of the mass spectral data of relevant literature and control substances led to the identification of 75 compounds, predominantly flavonoids, coumarins, and alkaloids, from ZXT extracts. To explore the therapeutic potential of ZXT in pneumonia treatment, network pharmacology and metabolomics techniques were employed to predict the associated targets and mechanisms of action for the aforementioned 75 compounds. In order to investigate the efficacy mechanism of ZXT in the treatment of pneumonia in more depth, this study used network pharmacology and molecular docking techniques to predict the targets and mechanisms of action associated with 75 identified compounds. Network pharmacology has

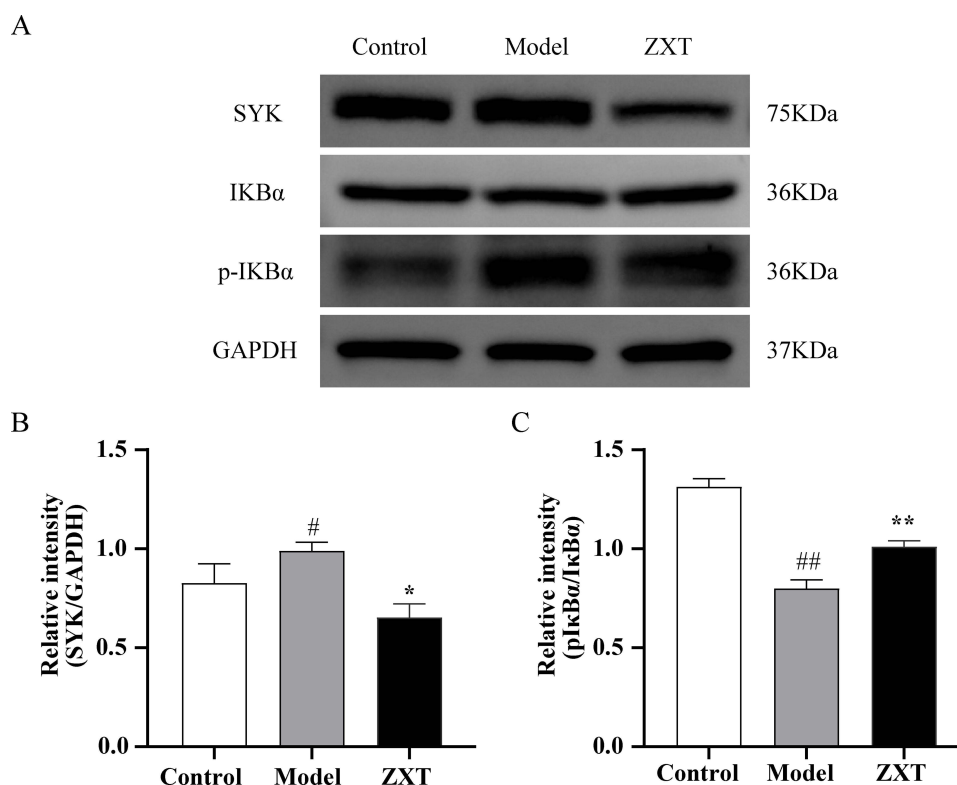


Figure 11 Effect of ZXT on the activation of Dectin-1 and SYK in 16HBE cells induced by LPS. **(A)** The protein expression of SYK, IκBα and pIκBα as determined by western blotting. GAPDH protein level was used as a loading control (n=3). Quantitative analysis of scanning densitometry for SYK **(B)** and IκBα **(C)**. #*p* < 0.05 and ##*p* < 0.01 versus the control group; **p* < 0.05 and ***p* < 0.01 versus the model group.

obvious advantages in predicting targets and potential mechanisms of action associated with ZXT. In addition, molecular docking can enhance the prediction of relationships between active ingredients and potential targets. Thus, the integration of these approaches proves to be advantageous in the study of active ingredients in TCM and the anticipation of their mode of operation.

The network pharmacological analysis revealed that ZXT primarily comprises ammidin, apigenin, and glabridin as its active compounds.^{23,24} Notably, ZXT exhibits a significant concentration within the signal pathway of the type C lectin receptor (CLR). It is important to acknowledge that CLR constitutes a protein superfamily distinguished by the presence of one or multiple type C lectin-like domains (CTLN). Dectin-1, a type C lectin receptor associated with the tyrosine-based activation motif (ITAM), is implicated in the initiation of intracellular signaling cascades that result in the synthesis of inflammatory cytokines and chemokines.¹⁸ Consequently, Dectin-1 assumes a crucial function in the activation of both innate and adaptive immune responses against pathogens. Research has demonstrated the involvement of Dectin-1 and SYK in the innate immune response to pneumonia. Dectin-1 mediates the recruitment of SYK via an activated ITAM motif, resulting in the phosphorylation and activation of SYK.²⁵ This subsequently regulates the generation of inflammatory cytokines associated with NF-κB downstream signaling, thereby exacerbating airway inflammation in pneumonia.

To comprehensively investigate the alterations in endogenous metabolites of 16HBE inflammation induced by ZXT, the mechanism underlying ZXT's efficacy in treating airway inflammation was examined through the integration of metabolomics and multivariate statistical analysis. Initially, the impact of ZXT on cell viability, inflammatory factor levels, and apoptosis in LPS-induced 16HBE cells was assessed to determine the optimal dosage. The experimental findings demonstrated that a concentration of 80 μg/mL of ZXT exhibited the most favorable activity, leading to a significant enhancement in cell viability and a reduction in the levels of inflammatory factors IL-4, IL-13, and TNF-α, as well as the apoptosis rate. Consequently, this particular concentration was chosen for further metabolomics analysis.

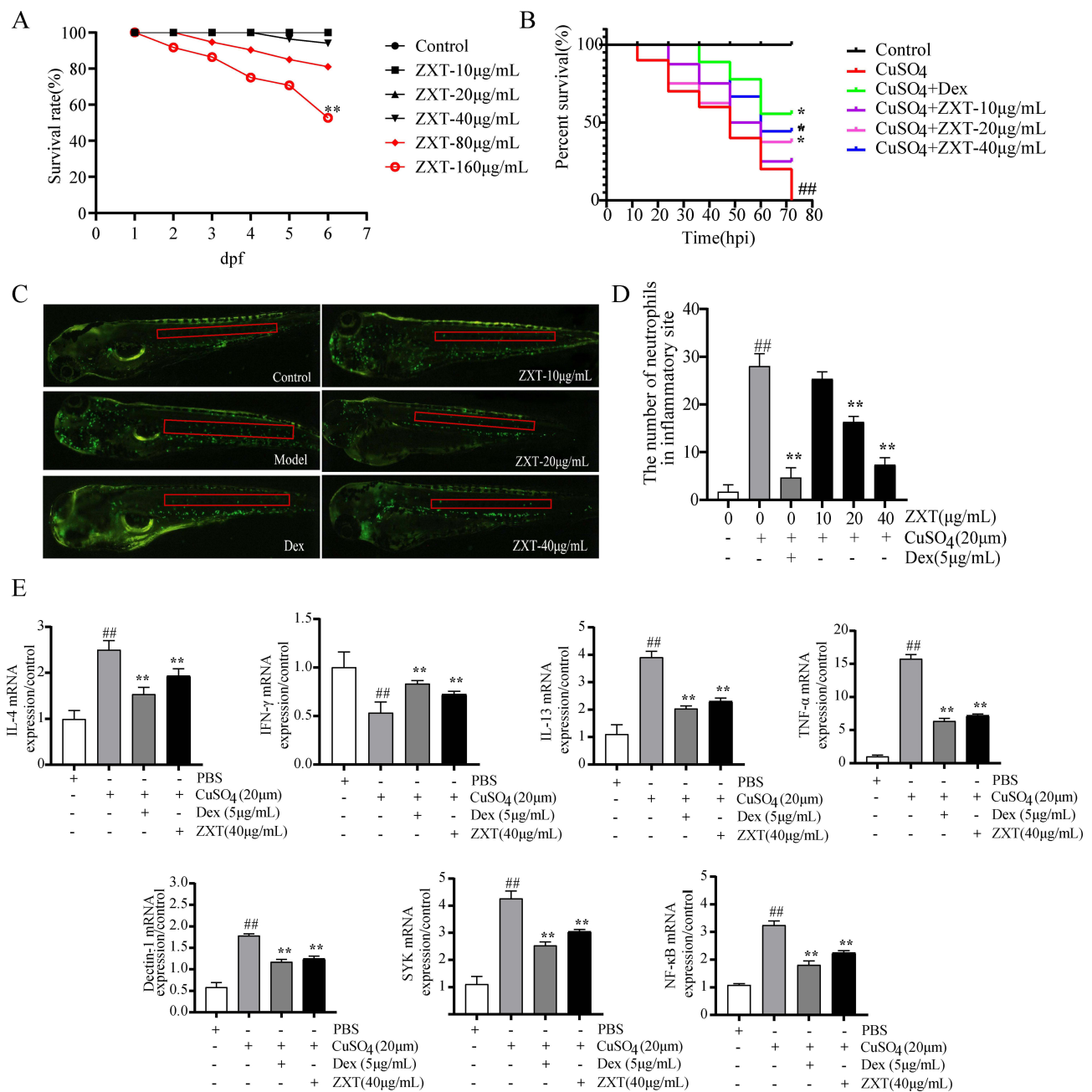


Figure 12 CuSO₄-induced inflammation in zebrafish is inhibited by ZXT. **(A)** The toxicity of ZXT in zebrafish. **(B)** The impact of ZXT on the survival rate of zebrafish stimulated with CuSO₄. **(C)** Effect of ZXT on neutrophil recruitment in zebrafish. **(D)** The neutrophils within the designated area were subjected to quantitative analysis. **(E)** Effects of ZXT on the mRNA expression levels of IL-4, IFN-γ, IL-13, TNF-α, Dectin-1, SYK, and NF-κB p65 in CuSO₄-stimulated zebrafish. Data are presented as the mean ± standard deviation (n = 5). [#]p < 0.05 and ^{##}p < 0.01 versus the control group; *p < 0.05 and **p < 0.01 versus the model group.

The findings of this study indicate that the intervention of ZXT resulted in significant up-regulation of valine, arginine, choline, betaine, retinol, and tyrosine, while 4-aminobutyric acid, hypoxanthine, histidine, malic acid, 1-O-ethyl-β-D-glucoside, inositol, and β-fructofuran were significantly down-regulated. Furthermore, the KEGG analysis revealed that the intervention primarily impacted amino acid metabolism, energy metabolism, protein biosynthesis, and other metabolic pathways.

Retinol serves as the precursor to retinoic acid, a bioactive metabolite of vitamin A found in various tissues, which exhibits anti-inflammatory and antioxidant properties.²⁶ In the presence of airway allergens, the absence of retinoic acid-related orphan receptor γt (RORγt) can diminish the immune response of Th2 cells and result in inflammation.²⁷ The

retinoic acid signal plays a crucial role in preserving the structure and function of airway smooth muscle, thereby mitigating eosinophilic airway inflammation and maintaining homeostasis through various mechanisms. In vivo, tyrosine is synthesized through the hydroxylation of phenylalanine, serving as a crucial precursor for hormone synthesis. A decrease in tyrosine levels subsequently hampers hormone production, thereby impacting pneumonia.²⁸ Research indicates that microbial metabolism of tyrosine exerts a protective influence on allergic airway inflammation, while its intestinal substitute, cresol sulfate, selectively diminishes chemokine ligands generated by airway epithelial cells, thereby safeguarding the host against damage caused by airway inflammation.²⁹ The decrease in tyrosine content subsequent to modeling led to a reduction in hormone synthesis, whereas the increase in tyrosine content following administration suggests that ZXT may contribute to enhanced hormone synthesis and diminished airway inflammation.³⁰ Histidine, an indispensable amino acid, is closely associated with inflammation and oxidative stress. Serving as a precursor to histamine, histidine assumes a crucial role in Th2 inflammatory response and airway smooth muscle contraction, thereby implying that histidine may serve as an indicator of Th2 inflammation as well. 4-Aminobutyric acid (also known as GABA) is a non-protein amino acid that is widely present in animals and plants.³¹ GABA serves as the primary inhibitory amino acid transmitter in the central nervous system. Its main functions are observed in the central nervous system, brain, and reproductive system. Additionally, GABA has been found to exist in airway smooth muscle cells, airway epithelial cells, and other surrounding tissues.³² This presence may be associated with allergen activation and involvement in airway remodeling, potentially leading to pneumonia. The overexpression of GABA in pneumonia leads to sustained depolarization of ciliated columnar epithelium and triggers metaplasia of goblet epithelial cells within the same epithelium, resulting in airway remodeling. This observation highlights the potential impact of the GABA system on various pathophysiological mechanisms involved in pneumonia development, thereby emphasizing its significant therapeutic value in pneumonia treatment. In conclusion, ZXT demonstrates the ability to restore the levels of certain differential metabolites to their normal state, thereby exerting a discernible “rectification” effect. This observation suggests that ZXT possesses the capacity to ameliorate the aberrant metabolic profile and substance metabolic disorder induced by LPS in bronchial epithelial cells, thus serving as a mechanism underlying its efficacy in the treatment of pneumonia.

Through the utilization of network pharmacology and metabolomics analysis, it has been determined that there exist four common targets, namely AKT1, SRC, MMP2, and SYK, among the ZXT target, pneumonia target, and metabolic target. Subsequent molecular docking analysis of these four targets has revealed that imperatorin, apigenin, and glabridin exhibit favorable binding affinity with crucial proteins. Consequently, the anti-inflammatory mechanism of ZXT has been substantiated via in vivo zebrafish experimentation and in vitro cell experiments. The primary characteristic of pneumonia is the presence of airway inflammation, primarily characterized by the infiltration of neutrophils. Implementing therapeutic measures to decrease the accumulation of neutrophils can serve as an effective approach to alleviate pneumonia symptoms. In this particular investigation, CuSO₄ was employed to induce acute inflammation in transgenic neutrophil fluorescent zebrafish, resulting in a substantial increase in neutrophil accumulation. Importantly, the administration of ZXT demonstrated a significant reduction in mortality among zebrafish stimulated with CuSO₄. Furthermore, administration of ZXT demonstrated a noteworthy reduction in neutrophil fluorescence, thereby suggesting its efficacious anti-inflammatory characteristics in vivo. Simultaneously, an investigation was conducted on the expression of IL-4, IFN- γ , IL-13, TNF- α , Dectin-1, SYK, and NF- κ B p65 genes in CuSO₄-induced zebrafish. The findings revealed that ZXT exhibited anti-inflammatory properties by impeding the activation of the Dectin-1/SYK/NF- κ B signaling pathway. Consistent experimental outcomes were also observed in in vivo cell experiments. The potential of ZXT to effectively diminish the nuclear translocation of NF- κ B, while concurrently suppressing the expression of Dectin-1 and SYK protein, will be investigated in a subsequent study utilizing a mouse animal model. This investigation aims to further explore the anti-inflammatory properties of ZXT and its potential association with the Dectin-1/SYK/NF- κ B pathway.

Conclusion

In summary, this study presents novel findings through a thorough examination of network pharmacology and metabolomics. The results demonstrate the notable anti-inflammatory properties of ZXT in both in vitro (16HBE cells) and in vivo (zebrafish) settings. Furthermore, the study successfully elucidates the potential therapeutic mechanism of pneumonia through the inhibition of the Dectin-1/SYK/NF- κ B pathway by ZXT. The aforementioned findings offer substantiation for the clinical utilization of ZXT in the treatment of pneumonia, thereby reinforcing the pivotal role of zebrafish in the realm of inflammation research.

Acknowledgments

This work was financially supported by the Jilin province science and technology development plan project (No. YDZJ202201ZYTS177), the National Natural Science Foundation of China (No. 82074127), the Administration of Traditional Chinese Medicine of Jilin Province Project (No.2022011) and the Jilin Province Development and Reform Commission (No.2023C027-2).

Disclosure

The authors report no conflicts of interest in this work.

References

- Jing XH, Zhao GY, Wang GB, et al. Naringin alleviates pneumonia caused by *Klebsiella pneumoniae* infection by suppressing NLRP3 inflammasome. *Biomed Pharmacother*. 2024;170:116028. doi:10.1016/j.biopha.2023.116028
- Zhu J, Dong X. Decursin alleviates LPS-induced lung epithelial cell injury by inhibiting NF- κ B pathway activation. *Allergol Immunopathol*. 2023;51(1):37–43. doi:10.15586/aei.v51i1.689
- Huang Z, Nie S, Wang S, et al. Therapeutic Effect of Costunolide in Autoimmune Hepatitis: network Pharmacology and Experimental Validation. *Pharmaceuticals (Basel)*. 2023;16(2):316. doi:10.3390/ph16020316
- Zhou C, Chen J, Zhang H, et al. Investigation of the chemical profile and anti-inflammatory mechanisms of flavonoids from *Artemisia vestita* Wall. ex Besser via targeted metabolomics, zebrafish model, and network pharmacology. *J Ethnopharmacol*. 2023;302(Pt B):115932. doi:10.1016/j.jep.2022.115932
- Liu Z, Huo JH, Dong WT, et al. A Study Based on Metabolomics, Network Pharmacology, and Experimental Verification to Explore the Mechanism of Qinbaqingfei Concentrated Pills in the treatment of *Mycoplasma Pneumonia*. *Front Pharmacol*. 2021;12:761883. doi:10.3389/fphar.2021.761883
- Lv JW, Li CN, Gao XC, et al. Screening of Active Ingredients of Bushen Zhuanggu Decoction for Promoting Testosterone Synthesis Based on 1H NMR Metabolomics Combined with Molecular Docking Technology. *Chin J Anal Chem*. 2021;49:779–788. doi:10.19756/j.issn.0253-3820.201583
- Zhang KY, Li CN, Zhang NX, et al. UPLC-QE-Orbitrap-Based Cell Metabolomics and Network Pharmacology to Reveal the Mechanism of N-Benzylhexadecanamide Isolated from Maca (*Lepidium meyenii* Walp.) against Testicular Dysfunction. *Molecules*. 2023;28(10):4064. doi:10.3390/molecules28104064
- Zheng Y, Tian C, Fan C, et al. Sheng-Mai Yin exerts anti-inflammatory effects on RAW 264.7 cells and zebrafish. *J Ethnopharmacol*. 2021;267:113497. doi:10.1016/j.jep.2020.113497
- Meng R, Wu S, Chen J, et al. Alleviating effects of essential oil from *Artemisia vulgaris* on enteritis in zebrafish via modulating oxidative stress and inflammatory response. *Fish Shellfish Immunol*. 2022;131:323–341. doi:10.1016/j.fsi.2022.10.010
- Ye Q, Zhang Q, Yao H, et al. Active-Ingredient Screening and Synergistic Action Mechanism of Shagan Mixture for Anti-Asthma Effects Based on Network Pharmacology in a Mouse Model of Asthma. *Drug Des Devel Ther*. 2021;15:1765–1777. doi:10.2147/DDDT.S288829
- Zhang FX, Li ZT, Yang X, et al. Discovery of anti-flu substances and mechanism of Shuang-Huang-Lian water extract based on serum pharmaco-chemistry and network pharmacology. *J Ethnopharmacol*. 2021;268:113660. doi:10.1016/j.jep.2020.113660
- Ma H, Fu W, Yu H, et al. Exploration of the anti-inflammatory mechanism of Lanqin oral solution based on the network pharmacology analysis optimized by Q-markers selection. *Comput Biol Med*. 2023;154:106607. doi:10.1016/j.compbiomed.2023.106607
- Wang L, Pu X, Nie X, et al. Integrated serum pharmacochemistry and network pharmacological analysis used to explore possible anti-rheumatoid arthritis mechanisms of the Shentong-Zhuyu decoction. *J Ethnopharmacol*. 2021;273:113988. doi:10.1016/j.jep.2021.113988
- Wei J, Yu Y, Zhang Y, et al. Integrated Serum Pharmacochemistry and Network Pharmacology Approach to Explore the Effective Components and Potential Mechanisms of Menispermi Rhizoma Against Myocardial Ischemia. *Front Chem*. 2022;10:869972. doi:10.3389/fchem.2022.869972
- Wang Y, Zou J, Jia Y, et al. The Mechanism of Lavender Essential Oil in the Treatment of Acute Colitis Based on "Quantity-Effect" Weight Coefficient Network Pharmacology. *Front Pharmacol*. 2021;12:644140. doi:10.3389/fphar.2021.644140
- Paudel KR, Panth N, Manandhar B, et al. Attenuation of Cigarette-Smoke-Induced Oxidative Stress, Senescence, and Inflammation by Berberine-Loaded Liquid Crystalline Nanoparticles: in Vitro Study in 16HBE and RAW264.7 Cells. *Antioxidants (Basel)*. 2022;11(5):873. doi:10.3390/antiox11050873
- Clyne A, Yang L, Yang M, May B, Yang AWH. Molecular docking and network connections of active compounds from the classical herbal formula Ding Chuan Tang. *PeerJ*. 2020;8:e8685. doi:10.7717/peerj.8685
- Hadebe S, Brombacher F, Brown GD. C-Type Lectin Receptors in Asthma. *Front Immunol*. 2018;9:733. doi:10.3389/fimmu.2018.00733

19. Corry DB, Rishi K, Kanellis J, et al. Decreased allergic lung inflammatory cell egression and increased susceptibility to asphyxiation in MMP2-deficiency. *Nat Immunol.* **2002**;3(4):347–353. doi:10.1038/ni773
20. Guo HW, Yun CX, Hou GH, et al. Mangiferin attenuates TH1/TH2 cytokine imbalance in an ovalbumin-induced asthmatic mouse model. *PLoS One.* **2014**;9(6):e100394. doi:10.1371/journal.pone.0100394
21. Gao XC, Zhang NX, Shen JM, et al. Screening of the Active Compounds against Neural Oxidative Damage from Ginseng Phloem Using UPLC-Q-Exactive-MS/MS Coupled with the Content-Effect Weighted Method. *Molecules.* **2022**;27(24):9061. doi:10.3390/molecules27249061
22. Qin X, Wu Y, Zhao Y, et al. Revealing active constituents within traditional Chinese Medicine used for treating bacterial pneumonia, with emphasis on the mechanism of baicalein against multi-drug resistant *Klebsiella pneumoniae*. *J Ethnopharmacol.* **2024**;321:117488. doi:10.1016/j.jep.2023.117488
23. Li J, Zhang B. Apigenin protects ovalbumin-induced asthma through the regulation of Th17 cells. *Fitoterapia.* **2013**;91:298–304. doi:10.1016/j.fitote.2013.09.009
24. Liu H, Xu RX, Gao S, Cheng AX. The Functional Characterization of a Site-Specific Apigenin 4'-O-methyltransferase Synthesized by the Liverwort Species *Plagiochasma appendiculatum*. *Molecules.* **2017**;22(5):759. doi:10.3390/molecules22050759
25. Pedroza LA, Kumar V, Sanborn KB, et al. Autoimmune regulator (AIRE) contributes to Dectin-1-induced TNF- α production and complexes with caspase recruitment domain-containing protein 9 (CARD9), spleen tyrosine kinase (Syk), and Dectin-1. *J Allergy Clin Immunol.* **2012**;129(2):464–72,472.e1–3. doi:10.1016/j.jaci.2011.08.027
26. Barbosa KC, Cunha DF, Jordão AA, Weffort VR, Cunha SF. Transient decreased retinol serum levels in children with pneumonia and acute phase response. *J Pediatr.* **2011**;Vol. 87(5): 457–460. doi:10.2223/JPED.2104
27. Xu Z, Bai S, Wu H, Fang M. Elevated retinal retinol-binding protein 4 levels in diabetic mice can induce retinal neurodegeneration through microglia. *Microsc Res Tech.* **2023**;86(2):223–231. doi:10.1002/jemt.24258
28. Xie S, Liang J, Zhao Y, et al. The second-generation tyrosine kinase inhibitor Afatinib inhibits IL-1 β secretion via blocking assembly of NLRP3 inflammasome independent of epidermal growth factor receptor signaling in macrophage. *Mol Immunol.* **2023**;153:135–145. doi:10.1016/j.molimm.2022.11.009
29. Tu H, Xiong W, Zhang J, Zhao X, Lin X. Tyrosine phosphorylation regulates RIPK1 activity to limit cell death and inflammation. *Nat Commun.* **2022**;13(1):6603. doi:10.1038/s41467-022-34080-4
30. Tian J, Dillion BJ, Henley J, Comai L, Kaufman DL. A GABA-receptor agonist reduces pneumonitis severity, viral load, and death rate in SARS-CoV-2-infected mice. *Front Immunol.* **2022**;13:1007955. doi:10.3389/fimmu.2022.1007955
31. Tian J, Middleton B, Kaufman DL. GABAA-Receptor Agonists Limit Pneumonitis and Death in Murine Coronavirus-Infected Mice. *Viruses.* **2021**;13(6):966. doi:10.3390/v13060966
32. Tian J, Middleton B, Kaufman DL. GABA administration prevents severe illness and death following coronavirus infection in mice. *bioRxiv.* **2020**. doi:10.1101/2020.10.04.325423

Journal of Inflammation Research

Dovepress

Publish your work in this journal

The Journal of Inflammation Research is an international, peer-reviewed open-access journal that welcomes laboratory and clinical findings on the molecular basis, cell biology and pharmacology of inflammation including original research, reviews, symposium reports, hypothesis formation and commentaries on: acute/chronic inflammation; mediators of inflammation; cellular processes; molecular mechanisms; pharmacology and novel anti-inflammatory drugs; clinical conditions involving inflammation. The manuscript management system is completely online and includes a very quick and fair peer-review system. Visit <http://www.dovepress.com/testimonials.php> to read real quotes from published authors.

Submit your manuscript here: <https://www.dovepress.com/journal-of-inflammation-research-journal>